Int. J. Electrochem. Sci., 17 **(2022)** Article Number: 220135, doi: 10.20964/2022.01.02

International Journal of
ELECTROCHEMICAL
SCIENCE
www.electrochemsci.org

Ethoxy-functional-group of polysiloxane coated high-nickel $LiNi_{0.80}Co_{0.15}Al_{0.05}O_2$ (NCA) composite cathode materials with excellent cycling stability

Zi Yang, Zhimin Li[*]

School of Advanced Materials and Nanotechnology, Xidian University, Xi'an 710071, P R China
[*]E-mail: zmli@mail.xidian.edu.cn

Received: 31 August 2021 / *Accepted:* 28 September 2021 / *Published:* 6 December 2021

Interfacial side reactions and HF erosion have been the most important challenges hindering the development of high-nickel $LiNi_{0.80}Co_{0.15}Al_{0.05}O_2$ (NCA) cathode material that is used in lithium-ion batteries. In the present study, a silicon-based coating, mainly consisting of ethoxy groups, is proposed to overcome issues of interfacial side reactions and HF erosion. The silicon-based coating is formed by in situ hydrolysis condensation between tetraethyl orthosilicate (TEOS) and trace amounts of water adsorbed on the surface of NCA. X-ray diffraction (XRD) analysis shows that TEOS treatment did not affect the crystal structure of NCA, which maintained a layered structure. Both the scanning electron microscopy (SEM) and transmission electron microscopy (TEM) confirmed that the polysiloxane protective shell was successfully formed on the surface of NCA particles, which could help avoid the direct contact between the active material and the electrolyte, and inhibit the interfacial side reactions. After 150 cycles at 1 C rate, the capacity retention was only 52.41%, whereas the capacity retention of NCA-3 was significantly higher and exemplary. The excellent cycling performance was due to the reason that the trace water was depleted due to the formation of ethoxy-functional-group of polysiloxane, which reduced the efficiency of interfacial reaction and improved the stability of interface by consuming HF.

Keywords: Lithium-ion battery; NCA; Coating; Cycling stability

1. INTRODUCTION

Recently, as a reliable energy storage and conversion system, lithium-ion batteries (LIBs) have been profoundly used in EVs, HEVs, PHEVs and other new applications. As one of the core components of LIBs, cathode materials have become the focus of research [1, 2]. Among the many cathode materials used in LIBs, layered $LiNi_{0.8}Co_{0.15}Al_{0.05}O_2$ (NCA) cathode material has attracted

significant attention due to favorable properties, such as excellent specific capacity, and stable cycling and rate performances. Although NCA cathode materials have shown outstanding electrochemical performance, they have certain drawbacks that need to be resolved [3-6]. For example, interfacial side reactions have a great impact on the long-term cycling efficiency of NCA cathode materials [7]. In continuous charge/discharge process, the active Ni^{3+} involved in the redox reaction will be oxidized to Ni^{4+} with strong oxidizability. Moreover, Ni^{4+} will accelerate the decomposition of electrolyte and form solid electrolyte interface (SEI) film on the surface of active particles, which block the path of Li^+ diffusion, and increase the polarization [8-10]. Secondly, as a high-nickel layered cathode material, the surface of NCA has high moisture absorption capability. The solute in the electrolyte is $LiPF_6$, which reacts with the trace water that inevitably remains on the surface of positive particles to form corrosive HF, which causes the surface structure of the active material to collapse and gradually spread inwards. In addition, cation mixing is also one of the key processes for the permanent capacity loss. Due to the similar radius, Ni^{2+} will occupy the position of Li^+ and form NiO passivation layer, resulting in irreversible capacity attenuation [11-13].

As the capacity-fading of NCA generally originates from the surface of particles, surface coatings have been extensively employed as a direct and effective strategy to relieve side reactions in electrolyte, prevent cathode material from HF erosion and stabilize the surface structure [14]. Therefore, plenty of materials have been adopted as surface coatings such as metal oxides (SiO_2, CeO_2, TiO_2, and Al_2O_3) [15-18], metal fluorides (AlF_3, and FeF_3) [19, 20], metal phosphates ($Ni_3(PO_4)_2$, $FePO_4$, and $Co_3(PO_4)_2$) [21-23], multiple oxides (Li_2O-ZrO_2, and Li_2O-$2B_2O_3$) [24, 25], carbon materials (graphene [26], and CNT [27]), and poly(3,4-ethylenedioxythiophene) (PEDOT) [28]. The essential purpose of a surface coating is to artificially protect the surface of the active material, directly isolate the contact between the active material and the electrolyte, inhibit the occurrence of side reactions and improve the stability of the surface structure. However, a good coating does not affect the diffusion of Li^+. Nevertheless, many surface modification materials are not very effective in removing HF that causes strong corrosion on the surface of NCA. Moreover, for NCA, the presence of $LiOH/Li_2CO_3$ and H_2O on the surface will accelerate the formation of HF, which results in structural instability and irreversible capacity attenuation of NCA at high temperature [29-31]. In short, an appropriate modified material should firstly protect the electrode from adverse reactions with the electrolyte, and secondly, the amount of water adsorbed on the surface of NCA particles should be minimum. Moreover, HF should also be easily removable from the electrolyte.

According to a previous study, Co_3O_4 has been coated onto $LiNi_{0.8}Co_{0.15}Al_{0.05}O_2$ surface using wet-coating method. The coating acted as a HF-scavenger and consumed LiOH during thermal treatment to enhance the surface structure and improve the electrochemical performance [32]. However, $LiNi_{0.8}Co_{0.15}Al_{0.05}O_2$ is significantly sensitive to water because of high nickel content [33]. Therefore, the formation of surface coating by precipitation will cause permanent damage to the surface structure of particles, and it becomes difficult to recover the damage caused in the early stage even if it can be treated by high temperature in the later stage [34]. Furthermore, high temperature treatment is a complex procedure, resulting in increased costs and damages to industrial production. Given this, it is important to look for an efficient modification material, which not only clears moisture on the surface without calcination, but also does not introduce additional H_2O. Tetraethyl orthosilicate

(TEOS) is rather sensitive to environment, that is to say, it is prone to hydrolysis and condensation polymerization in alkaline or acidic conditions [35]. TEOS is usually used as an additive in lithium batteries. To a certain extent, it can promote the formation of SEI film on the surface of particles, prevent the dissolution of transition metal ions from causing structure collapse, thus inhibiting the insecurity caused by gas generation and improving the cycling performance [36]. Additionally, it is reported that TEOS hydrolyzes to generate polysiloxane, which is vital to removing HF [37]. However, TEOS has rarely been reported in the field of NCA either as an additive or as a precursor to introducing ethoxy functional groups [38].

In this paper, a protective polysiloxane coating is grown on the surface of NCA particles using a simple interfacial hydrolyzation-condensation technique. Under the condition of no heating, TEOS can spontaneously hydrolyze with trace water remaining on the surface of NCA, condense, and finally form homogeneous polysiloxane coating on the surface of NCA particles. After polysiloxane modification, the capacity retention of NCA was significantly improved in the long-term cycle.

2. EXPERIMENTAL

The NCA powder was synthesized using a sol-gel method. The sol was formed at 80 °C by mixing $LiNO_3$, $Ni(NO_3)_2{\cdot}6H_2O$, $Co(NO_3)_2{\cdot}6H_2O$, and $Al(NO_3)_3{\cdot}9H_2O$ (n_{Li}:n_{Ni}:n_{Co}:n_{Al} = 1.07:0.8:0.15:0.05) with a certain amount of citric acid in the deionized water while heating to evaporate part of water with continuous stirring. Then, the sol was dried at 80 °C to form a dried gel. After that, the gel was fired in a tube furnace at 450 °C for 4 h, and calcined at 750 °C for 12 h with a heating rate of 10 °C min^{-1} under an oxygen atmosphere. In order to synthesize polysiloxane coating material, trace TEOS (n_{TEOS}:n_{NCA} = 0.03:1) was thoroughly dispersed in 50 mL ethanol under ultrasonic treatment and vigorous stirring, accompanied by the addition of 0.5 g of obtained pure NCA powder. The mixture was continuously stirred under 30 °C until the ethanol was adequately evaporated. The final product was the polysiloxane coated NCA, and called NCA-3.

The active substance, conductive agent (Super-P carbon) and binder (polyvinylidene fluoride) were mixed and dissolved in N-methyl-2-pyrrolidone in a mass ratio of 8:1:1. The slurry was painted onto the aluminum foil, and dried at 120 °C for 12 h. The cathode plate was assembled into a CR2016 coin-type battery in a glove box filled with argon gas. Half cells using metallic lithium anode, Celgard 2325 separator and 1M $LiPF_6$ carbonate electrolyte with ethylene carbonate (EC)/dimethyl carbonate (DMC)/diethyl carbonate (DEC) (1:1:1 in volume ratio).

The X-ray diffraction (XRD, D8 Advance, Bruker, Germany) analysis was conducted using Cu Kα as the radiation source, and used to detect the crystalline phases of obtained powder over the 2θ range of 10 - 80°. The morphology of the sample was observed using field emission scanning electron microscope (FESEM, JEOL, JSM-7500F, Japan). Moreover, energy-dispersive X-ray spectrometry (EDS) and transmission electron microscopy (TEM, JEM-2100F, JEOL, Japan) were adopted to observe the morphologies and microstructures of the samples. The specific surface areas and pore size distributions of the samples were measured using the Brunauer-Emmett-Teller (BET, AUTOSORB-IQ) technique. The electrochemical performance was assessed by galvanostatic charge-discharge on a

LAND system (CT2001A, LANHE, China) at 25 ºC. Cyclic voltammetry (CV) and electrochemical impedance spectroscopy (EIS) were obtained within the frequency range of 100 kHz - 0.1 Hz using a workstation (CHI660E, CHENHUA, China).

3. RESULTS AND DISCUSSION

In order to demonstrate the crystal structure and the formation of NCA and NCA-3 composites, XRD analysis was conducted. Fig. 1 shows the XRD patterns of the samples. Compared to the PDF card (JCPDS: No.74-0919), the diffraction peaks of both NCA and NCA-3 samples were indexed to a well-defined hexagonal α-$NaFeO_2$ layered structure (Space group: R-3m, 166) [39]. After the modification of NCA with polysiloxane, the peak strength and position of NCA-3 sample did not change significantly, indicating that polysiloxane had no effect on the crystal structure of NCA. Furthermore, there were no distinct differences in the lattice constants for NCA (a=2.8775 Å, c=14.1884 Å) and NCA-3 (a=2.8778 Å, c=14.1893 Å) estimated by Jade. All samples obviously exhibited two splitting peaks of $I_{(006)/(102)}$ and $I_{(108)/(110)}$, which proved a well-organized layer structure in the same way [40]. In general, the value of *c*/*a* was used to measure the layered structure of the sample, and the relative size of $I_{(003)}/I_{(104)}$ was used to determine the degree of cation mixing [41]. Furthermore, as defined by Reimers, the ratio of $[I_{(006)}+I_{(012)}]/I_{(101)}$ indicated the cation mixing. The lower the ratio, the better the hexagonal layered structure [42]. As expected, after the TEOS treatment, the value of c/a and $I_{(003)}/I_{(104)}$ or the ratio of $[I_{(006)}+I_{(012)}]/I_{(101)}$ had no significant change because the TEOS modification did not affect the crystal structure, thereby maintaining a good layered structure of the material. Additionally, there were no diffraction peaks indexed to polysiloxane according to the XRD pattern because of the amorphous state or low coating content [36]. These results once again prove that the polysiloxane coating had no significant effect on the main crystal phase and cation mixing of NCA cathode materials. Table 1 lists the corresponding data.

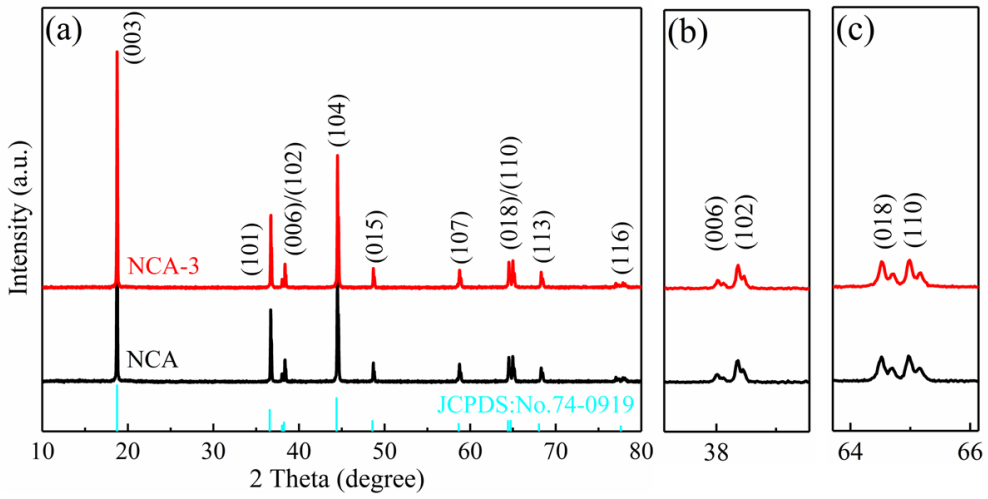

Figure 1. (a) XRD patterns; (b) zoomed-in XRD patterns of NCA and NCA-3 powders.

Table 1. Structural parameters of NCA and NCA-3.

Sample	Lattice parameters			$I_{(003)}/I_{(104)}$	$[I_{(006)}+I_{(012)}]/I_{(101)}$
	a (Å)	c (Å)	c/a		
NCA	2.8775	14.1884	4.9463	1.2278	0.4407
NCA-3	2.8778	14.1893	4.9461	1.2281	0.4413

SEM and EDS measurements were performed to verify the existence and distribution of polysiloxane coating on the material surface. Fig. 2(a) and 2(b) show the SEM images of NCA and NCA-3 samples prepared using sol-gel method, respectively. For NCA and NCA-3 samples, all of them were irregularly shaped blocks agglomerated by small particles, and there was no obvious difference in the morphology of the samples. However, the FESEM map of the TEOS-treated NCA-3 sample showed that the surface of the particles was markedly rough, which may have been caused by the polysiloxane coating. Meanwhile, compared with the NCA particles, the particle shape of NCA-3 sample also tended to be spherical, which is chain organic polymer, and induced particle-to-spherical aggregation during in-situ polymerization.

It has been reported that spherical particles are beneficial to the cathode materials to maintain good cycling performance during charging and discharging. In order to determine the composition, EDS elemental mapping of NCA-3 particles is shown Fig. 2(d) - 2(h). The results show that, in addition to Ni, Co, Al and O elements, Si element also existed in the system. The distribution of Si element was the same as that of other elements, which were homogeneously distributed. These results confirm that polysiloxane had been successfully coated on the surface of NCA particles very uniformly.

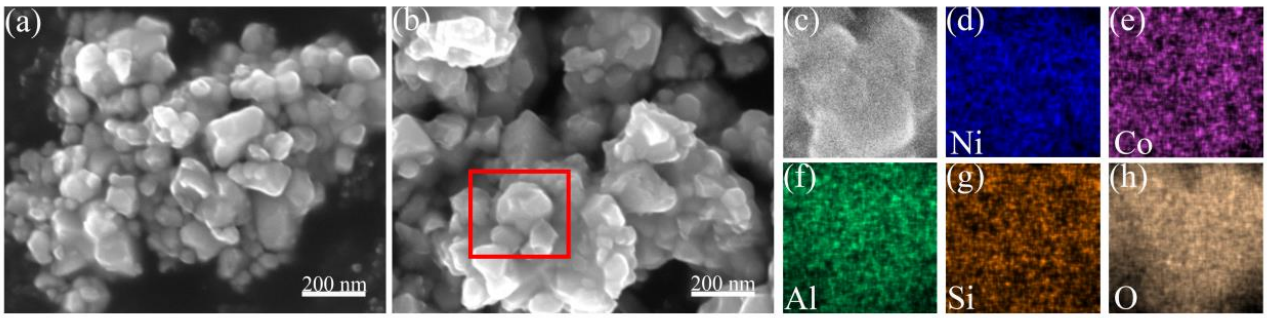

Figure 2. SEM images of (a) NCA and (b) NCA-3 samples; EDS elemental mapping of (c-h) NCA-3 particle.

TEM tests were used to visually observe the coating. Fig. 3(a) shows the representative TEM image of NCA-3 sample. TEM image of NCA-3 clearly shows that the particles had a core-shell structure. The modification material acted as a protect shell, correspondingly, NCA acted as an active nucleus. It is apparent that the coating was approximately 20 nm thick and had a uniform presence on

the surface of particles. Similar to the SEM image, the mapping plots for Ni, Co, Al, Si and O are shown in Fig. 3(c) - 3(g). In addition, the results show that the distribution of these elements in the region was very uniform. According to the EDS line sweep, from the outside to the inside, the distribution of silicon element was high to low, whereas that of nickel element was from low to high, further indicating that the silicon element was uniformly distributed in the shell layer, whereas the inside was a high nickel cathode material. This also proves that, after the TEOS treatment, a uniform protective layer was developed on the surface of the cathode material.

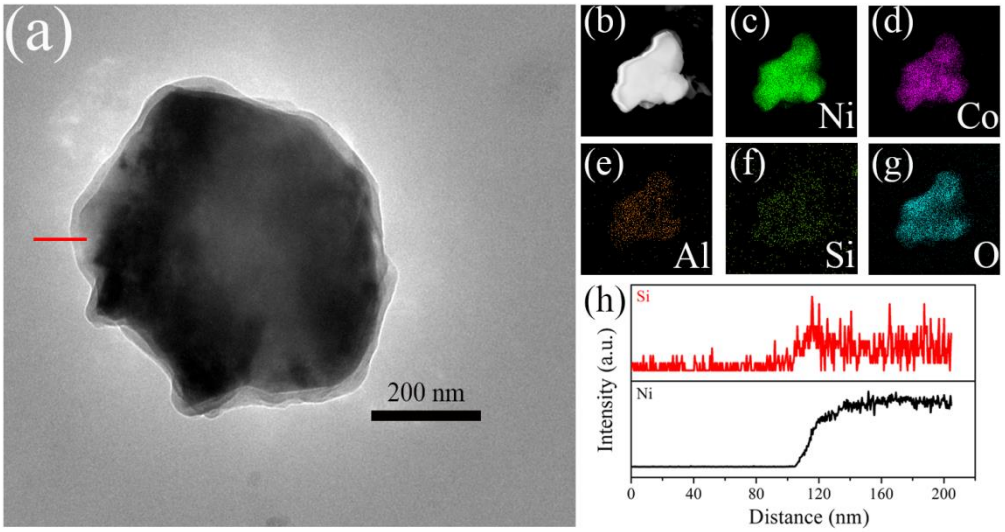

Figure 3. (a) TEM images of NCA-3 sample; (b-g) EDS elemental mapping images of NCA-3 particle; (h) Grain edge element distribution diagram.

The nitrogen adsorption/desorption isotherms and the Barrett Joyner-Halenda (BJH) curves are shown in Fig. 4. According to the International Union of Pure and Applied Chemistry (IUPAC), the isotherms of both NCA and NCA-3 exhibited the typical irreversible Type III characteristics with a distinct H3 hysteresis loop [43, 44]. For the NCA cathode, the desorption isotherms diverged at $P/P_0 <$ 0.2, indicating a structural transformation or chemical reaction in the region [45, 46]. The specific surface areas of NCA and NCA-3 are listed in Table 2. The BET results were consistent with those of the SEM images, clarifying that the particle size of NCA-3 was smaller than that of NCA. Correspondingly, the results from the BET analysis revealed that the specific surface area of NCA-3 (19.018 m^2 g^{-1}) was remarkably larger than that of the NCA (1.088 m^2 g^{-1}), which was due to the special growth mechanism of chain polysiloxane, forming a chain-like porous structure during in-situ polymerization, and demonstrating that the polysiloxane polymerized in-situ on the surface of NCA and substantially decreased the side reactions [47]. At the same time, it can be further seen from the aperture distribution diagram in Fig. 4b that the NCA-3 sample had a relatively large specific surface area, which was conducive to the penetration of electrolyte during charging and discharging, and provided better reaction kinetics for the transmission of Li^+ [48].

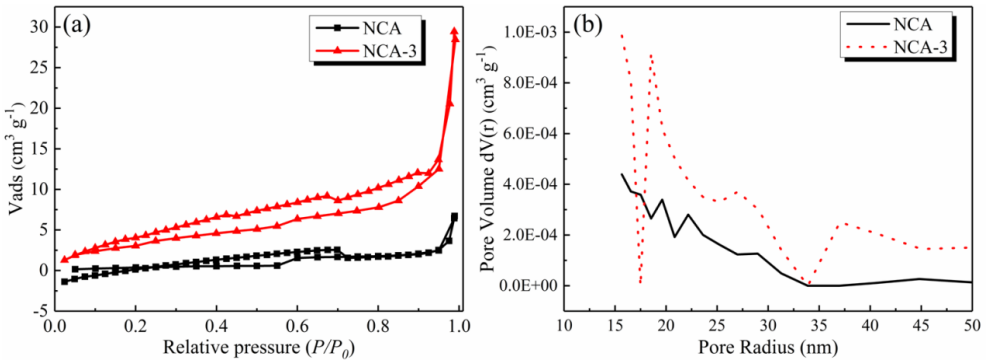

Figure 4. (a) Nitrogen absorption/desorption isotherms; (b) Pore size distributions for the samples.

Table 2. BET results of NCA and NCA-3 composites.

Sample	NCA	NCA-3
Specific surface area (m^2 g^{-1})	1.088	19.018
Pore Volume (cm g^{-1})	0.012	0.043

The initial charge/discharge performances of NCA and NCA-3 cathodes at 1/10 C are shown in Fig. 5a. In the overall shape and trend of the profiles, TEOS-modified NCA-3 sample did not undergo additional redox reaction during the charging and discharging. The initial discharge capacities of NCA and NCA-3 were 189.5 and 189.3 mAh g^{-1}, whereas the initial coulombic efficiency values were 83.14% and 83.83%, respectively. The irreversible capacity loss during the charging and discharging process were caused by the absence of oxygen and the formation of spinel phase on the surface [34]. Because the stoichiometric ratio of NCA is difficult to achieve, it is difficult to avoid the oxygen deficiency and cation mixing in the material during high temperature roasting. This will lead to the structural transformation of NCA from hexagonal layered structure to spinel structure and cubic rock salt structure. This structural decay is irreversible, generally from the surface of the material to the internal development. Compared with the NCA cathode, the irreversible capacity attenuation of TEOS-modified NCA-3 cathode was not significantly different from that of the NCA cathode, which had the values of 36.6 and 38.4 mAh g^{-1}, respectively. This is because, although polysiloxane coating can inhibit the occurrence of side reactions to a certain extent, it will affect the initial discharge capacity due to the reason that polysiloxane is non-conductive. Fig. 5b reveals the rate capabilities of NCA and NCA-3. When at a small rate, the discharge capacities of NCA and NCA-3 cathodes were almost the same. However, the discharge capacity of NCA-3 cathode was smaller than that of NCA cathode under high multiplier. The average discharge capacity of NCA and NCA-3 were 189.6 and 189.1 mAh g^{-1} at 0.1 C and 114.4 and 103.5 mAh g^{-1} at 5 C, respectively, indicating capacity retentions of 60.34% and 54.74%, respectively. This is mainly due to the reason that polysiloxane was not conductive and reduced the electronic conductance while increasing the interfacial resistance.

The cycling performance of NCA and NCA-3 cathodes are shown in Fig. 5c. The discharge capacity of NCA cathode decreased significantly with the continuous cycle. After 150 long cycles, the

capacity retention was only 52.41%. More interestingly, the TEOS modified sample showed a slight decrease in performance. However, as the number of cycles increased, the capacity increased and the cycle stability gradually increased. This is because the process of cycling was an active process. The presence of polysiloxane coating layer effectively inhibited the occurrence of interfacial side reactions, alleviated the growth of SEI film and enhanced cycle stability. In general, when non-conductive materials are used for coating, although protective skin can be formed on the surface of particles, it also inhibits the migration of Li^+ to a certain extent. Moreover, as the charge/discharge test was carried out, the polysiloxane coated on the surface of NCA particles fell off to a certain extent, and reacted with HF. As a result, a harmful substance was generated in the electrolyte, which inhibited the formation of SEI film.

In short, after the TEOS treatment, the stability of pure NCA sample was enhanced, because the polysiloxane coating layer could react with HF in the electrolyte and suppressed the accumulation of a thick SEI film. Additionally, the polysiloxane coating layer played a role of a barrier protecting the NCA from the electrolyte, thereby improving the cyclic performance.

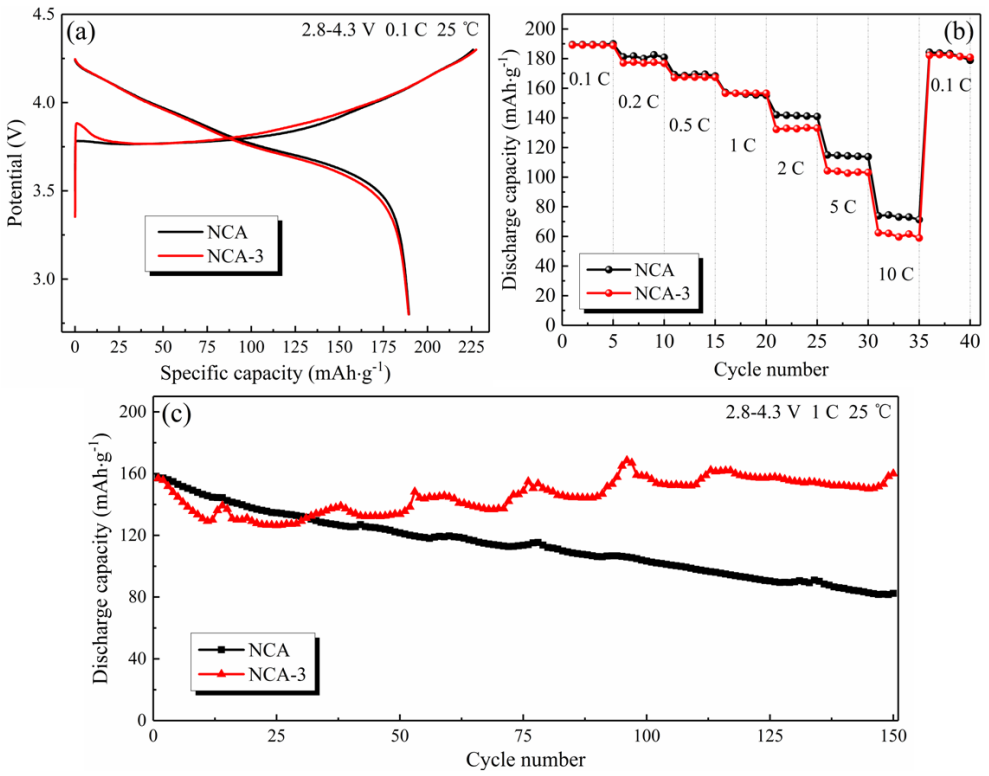

Figure 5. (a) Initial charge/discharge curves of NCA and NCA-3; (b) rate capability under variable current rate; (c) cycling performance at the current rate of 1 C.

In order to further evaluate the electrochemical stability of NCA and NCA-3 cathodes, cyclic voltammograms tests were carried out within the 2.2-4.6 V voltage range at a scan rate of 0.1 mV s^{-1}, as shown in Fig. 6. A careful comparison of the CV curves of the two samples shows that there were no redundant peaks except for the three pairs of similar redox peaks. This indicates that the polysiloxane coating had no effect on the redox reactions. The CV curves of both the NCA and NCA-3

reveal three pairs of redox peaks, corresponding to phase transitions of hexagonal (H1) to monoclinic (M), monoclinic to hexagonal (H2), and hexagonal (H2) to hexagonal (H3) during the Li^+ extraction/insertion in active materials [49, 50]. Oxidation peaks of NCA and NCA-3 were observed at the voltages of 3.98 V and 3.93 V at the 1st cycle and obviously shifted to lower voltages of 3.82 V and 3.79 V at the second cycle, respectively. These results further show that there was an irreversible electrochemical reaction during the first cycle [51]. It can be further seen that, in the second cycle, the potential difference of the REDOX peak of NCA cathode was 0.15 V, while the potential difference of the corresponding NCA-3 was 0.12 V. The voltage difference value is often used to represent the cyclic performance. The smaller the voltage difference, the smaller the capacity loss during the cycle and the better the cyclic stability. The cathode of NCA-3 had a smaller potential difference, which shows that the redox reaction in the charging and discharging process was more reversible. Furthermore, the polarization phenomenon was smaller, and the cycling stability was better. More significantly, the capacity retention of NCA-3 was higher than the values reported in some recent reports of other coating materials, such as, TiO_2, Al_2O_3, $FePO_4$, Li_2O-ZrO_2, SnO_2, MnO_2, AlF_3, and $LiTiO_2$ (see Table 3).

Table 3. A comparison of cycling performances of various coating materials.

Sample	Al_2O_3	$FePO_4$	Li_2O-ZrO_2	SnO_2	MnO_2	AlF_3	$LiTiO_2$
Capacity retention rate (%)	90.4	88.3	80.0	86.2	88.7	88.1	90.8
Ref.	[17]	[22]	[24]	[52]	[53]	[19]	[54]

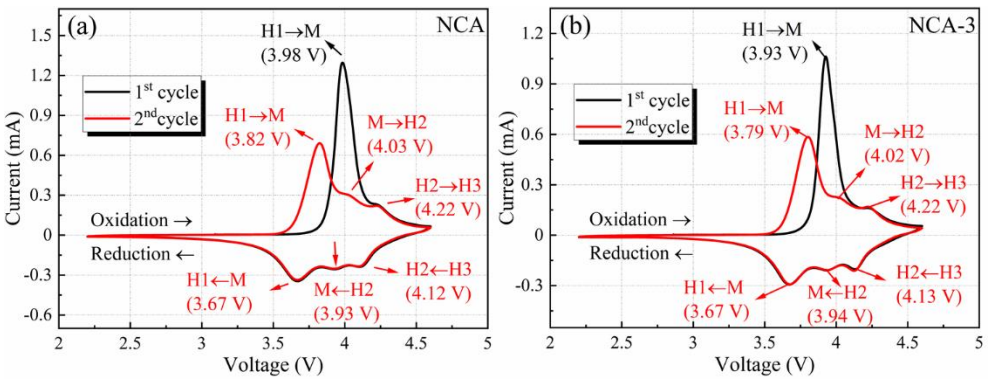

Figure 6. Cyclic voltammetry curves of (a) NCA and (b) NCA-3 cathode over 2.2- 4.6 V.

In order to explore the influence of polysiloxane coating on the structural stability of NCA, EIS tests were conducted on the fresh and 150 cycles of NCA and NCA-3 cells, respectively, and the corresponding results are shown in Fig. 7.

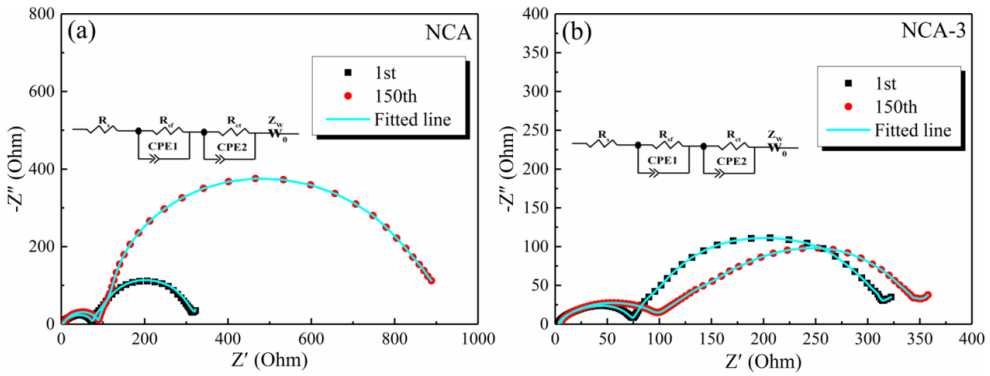

Figure 7. Nyquist plots of (a) NCA and (b) NCA-3 samples before cycling and after 150 cycles. The inset shows the equivalent circuit.

Table 4. Fitting resistance values of NCA and NCA-3 samples.

Sample	Uncirculated		150th cycle	
	R_{ct} (Ω)	R_{sf} (Ω)	R_{ct} (Ω)	R_{sf} (Ω)
NCA	72.41	249.20	87.75	808.70
NCA-3	72.66	247.10	94.91	268.50

The impedance spectra were fitted using equivalent circuit models, including three parts, which consisted of two semicircles and a line. A semicircle in the high frequency region corresponds to the interface impedance, while a semicircle in the intermediate frequency region corresponds to the charge transfer impedance, which is related to the electron transfer between the interfaces. The line in the low frequency region corresponds to the resistance in the Li^+ diffusion process [55]. The detailed fitting resistance values are presented in Table 4. The R_{ct} of NCA-3 (72.66 Ω) cathode after the 1st cycle was slightly larger than that of NCA (72.41 Ω) cathode. This is because the polysiloxane coating was organic and nonconductive, so the electronic conductivity was very poor, thus increasing the resistance. Interestingly, the R_{sf} of NCA cathode increased from 247.10 Ω at first cycle to 808.70 Ω at the 150th cycle at 1 C, while the growth (from 247.10 to 268.5 Ω) of R_{sf} of NCA-3 cathode obviously decreased after 150 cycles. This was due to the ethoxyl functional groups gradually shedding during the cycling process, creating a channel more suitable for Li^+ transmission. In short, the polysiloxane can significantly inhibit the resistance during the cycling process, thus improving the cycling stability.

4. CONCLUSIONS

A uniform protective layer was evenly deposited on the surface of NCA cathode particles using in-situ hydrolysis and condensation of TEOS without heat treatment. The results show that the NCA cathode materials coated with polysiloxane had a good capacity retention under long-term circulation. During the modification process of TEOS hydrolysis and polycondensation, the trace H_2O was consumed, leading to reduced production of HF. The polysiloxane coating acted like a barrier, which

alleviated the occurrence of interfacial side reactions. After 150 cycles at 1 C rate, NCA-3 sample revealed extremely high capacity retention compared to that of NCA sample. Consequently, as an artificial skin protection, the polysiloxane plays an important role in inhibiting the interfacial reaction. It can prevent the electrolyte from permeating into the middle of particles, slow down the HF's erosion on the active material, and help remove HF from the surface. This provides an effective and energy-saving way for preparing high energy density LIB cathodes.

References

1. C. Liu, J. Yuan, R. Masse, X. Jia, W. Bi，Z. Neale, T. Shen, M. Xu, M. Tian, J. Zheng, J. Tian, G. Cao, *Adv. Mater*., 33(22) (2020) 1905245.
2. E. Pomerantseva, F. Bonaccorso, X. Feng, Y. Cui, Y. Gogotsi, *Science*, 366 (2019) 6468.
3. S.J. Zheng, R. Huang, Y. Makimura, Y. Ukyo, C. Fisher, T. Hirayama, Y. Ikuhara, *J. Electrochem. Soc.*, 158(4) (2011) A357.
4. S. Watanabe, M. Kinoshita, K. Nakura, *J. Power Sources*, 247 (2014) 412-422.
5. S. Hwang, W. Chang, S.M. Kim, D. Su, D.H. Kim, J.Y. Lee, K.Y. Chung. E.A. Stach, *Chem. Mater*., 26(2) (2014) 1084-1092.
6. N. Faenza, Z. Lebens-Higgins, P. Mukherjee, S. Sallis, G. Amatucci, *Langmuir,* 33(37) (2017) 9333-9353.
7. L.W. Liang, W.H. Zhang, F. Zhao, D.K. Denis, F.U. Zaman, L.R. Hou, C.Z. Yuan, *Adv. Mater. Interfaces*, 7.3 (2020).
8. S. Watanabe, M. Kinoshita, K. Nakura, *J. Power Sources*, 247 (2014) 412-422.
9. N. Faenza, Z. Lebens-Higgins, P. Mukherjee, S. Sallis, N. Pereira, F. Badway, A. Halaijko, G. Ceder, F. Cosandey, L. Piper, G. Amatucci, *Langmuir*, 33.37 (2017) 9333-9353.
10. S. Muto, Y. Sasano, K. Tatsumi, T. Sasaki, K. Horibuchi, Y. Takeuchi, Y. Ukyo, *J. Electrochem. Soc.*, 156.5 (2009) A371-A377.
11. W. Liu, P. Oh, X. Liu, M.J. Lee, W. Cho, S. Chae, Y. Kim, J. Cho, *Angew. Chem. Int. Ed*., 54.15 (2015) 4440-4457.
12. M.D. Radin, S. Hy, M. Sina, C.C. Fang, H.D. Liu, J. Vinckeviciute, M.H. Zhang, M.S. Whittingham, Y.S. Meng, A. Ven, *Adv. Energy Mater*., 7.20 (2017) 1602888
13. P.F. Yan, J.M. Zheng, J.G. Zhang, C.M. Wang, *Nano Lett*., 17.6 (2017) 3946-3951.
14. X.X. Yan, L. Chen, S.A. Shah, J.J. Liang, Z.F. Liu, *Electrochim. Acta*, 249 (2017) 179-188.
15. W. Shin, J. Yoo, W. Choi, *J. Mater. Chem*. A, 3(23) (2015) 12163-12170.
16. Y. Wu, A. Manthiram, *Solid State Ionics*, 180(1) (2009) 50-56.
17. Y. Xu, X.H. Li, Z.X. Wang, H.J. Guo, B. Huang, *Mater. Lett*., 143 (2015) 151-154.
18. K. Du, H.B. Xie, G.R. Hu, Z.D. Peng, Y.B. Cao, F. Yu, *ACS Appl. Mater. Interfaces*, 8(27) (2016) 17713-17720.
19. S. Lee, C. Yoon, K. Amine, Y. Sun, *J. Power Sources*, 234 (2013) 201-207.
20. W.M. Liu, X. Tang, M.L. Qin, G.L. Li, J.Y. Deng, X.W. Huang, *Mater. Lett*., 185 (2016) 96-99.
21. D.J. Lee, B. Scrosati, Y.K. Sun, *J. Power Sources*, 196(18) (2011) 7742-7746.
22. B. Huang, X.H. Li, Z.X. Wang, H.J. Guo, *Mater. Lett*., 131 (2014) 210-213.
23. Y.R. Bak, Y. Chung, J. Ju, M.J. Hwang, Y. Lee, K.S. Ryu, *J. New Mater. Electrochem. Syst*., 14(4) (2011) 203-207.
24. S. Ito, S. Fujiki, T. Yamada, Y. Aihara, Y. Park, T.Y. Kim, S.W. Baek, J.M. Lee, S. Doo, N. Machida, *J. Power Sources*, 248 (2014) 943-950.
25. S.N. Lim, W. Ahn, S.H. Yeon, S.B. Park, *Electrochim. Acta*, 136 (2014) 1-9.
26. S. Yoon, K.N. Jung, S.H. Yeon, C.S. Jin, K.H. Shin, *J. Electroanal. Chem*., 683 (2012) 88-93.
27. L.P. Zhang, J. Fu, C.H. Zhang, *Nanoscale Res. Lett*., 12(1) (2017) 376.
28. G.L. Xu, Q. Liu, K.K.S. Lau, Y.Z. Liu, X. Liu, H. Gao, X.W. Zhou, M.H. Zhuang, Y. Ren, J.D. Li,

M.H. Shao, M.G. Ouyang, F. Pan, Z.H. Chen, K. Amine, G.H. Chen, *Nat. Energy*, 4.6 (2019) 484-494.
29. H. Visbal, S. Fujiki, Y. Aihara, T. Watanabe, Y. Park, S. Doo, *J. Power Sources*, 269 (2014) 396-402.
30. G.R. Zhuang, G.Y. Chen, J. Shim, X.Y. Song, P.N. Ross, T.J. Richardson, *J. Power Sources*, 134(2) (2004) 293-297.
31. O. Haik, N. Leifer, Z. Samuk-Fromovich, E. Zinigrad, B, Markovsky, L. Larysh, Y. Goffer, G. Goobes, D. Aurnach, *J. Electrochem. Soc*., 157(10) (2010) A1099.
32. Y.Q. Huang, Y.H. Huang, X.L. Hu, *Electrochim. Acta*, 231 (2017) 294-299.
33. S.W. Song, G.V. Zhuang, P.N. Ross, *J. Electrochem. Soc*., 151(8) (2004) A1162.
34. G.L. Tian, K.Y. Shu, C. Xiang, D.X. Zuo, *J. Alloys Compd*., 706 (2017) 24-40.
35. H.T. Pu, F.J. Jiang, Z.L. Yang, *Mater. Lett*., 60(1) (2006) 94-97.
36. Z. Wang, Y.D. Huang, X.C. Wang, X.C. Jia, D.Z. Jia, Z.P. Guo, M. Miao, *Solid State Ionics*, 232 (2013) 19-23.
37. H. Wang, W. Ge, W. Li, F. Wang, W. Liu, M.Z. Qu, G. Peng, *ACS Appl. Mater. Interfaces*, 8(28) (2016) 184 39-49.
38. S. Yamaguchi, H. Kagawa, K. Gen, K. Okuzawa, M. Matsuyama, *Aquaculture*, 239(1-4) (2004) 485-496.
39. L. Tan, H.W. Liu, *Solid State Ionics*, 181(33-34) (2010) 1530-1533.
40. S.H. Ju, H.C. Jang, Y.C. Kang, *Electrochim. Acta*, 52(25) (2007) 7286-7292.
41. W.S. Yoon, K.Y. Chung, J. Mcbreen, X.Q. Yang, *Electrochem. Commun*., 8(8) (2006) 1257-1262.
42. J.N. Reimers, J.R.Dahn, *J. Electrochem. Soc*., 139(8) (1992) 2091.
43. W.B. Hua, X.D. Guo, Z. Zheng, Y.J. Wang, B.H. Zhong, B.Z. Fang, J.Z. Wang, S.L. Chou, H. Liu, *J. Power Sources*, 275 (2015) 200-206.
44. W.Y. Liu, W.B. Hua, Z. Zheng, B.H. Zhong, Z.Y. Zhang, *Solid State Ionics*, 22(10) (2016) 1781-1790.
45. Y.X. Huang, C. Yan, X. Shi, W. Zhi, Z.M. Li, Y.Y. Yan, M.L. Zhang， G.Z. Cao, *Nano Energy*, 48 (2018) 430-440.
46. X.L. Zhang, F.Y. Cheng, K. Zhang, Y.L. Liang, S.Q. Yang, J. Liang, *J. Chen, RSC Adv*., 2(13) (2012) 5669.
47. X.J. Zhang, W.H. Shi, J.X. Zhu, W.Y. Zhao, J. Ma, S. Mhaisalkar, T.L. Maria, Y.H. Yang, H. Zhang, H.H. Hng, Q.Y. Yan, *Nano Res*., 3(9) (2010) 643-652.
48. L. Li, L. Wang, X.X. Zhang, M. Xie, F. Wu, R.J. Chen, *ACS Appl. Mater. Interfaces*, 7(39) (2015) 219 39-47.
49. B. Huang, X.H. Li, Z.X. Wang, H.J. Guo, X.H. Xiong, *Ceram. Int*., 40(8) (2014) 13223-13230.
50. H.J. Noh, S. Youn, C.S. Yoon, Y.K. Sun, *J. Power Sources*, 233 (2013) 121-130.
51. H. Buqa, A. Würsig, J. Vetter, M.E. Spahr, F. Krumeich, P. Novak, *J. Power Sources*, 153(2) (2006) 385-390.
52. Z.C. Xie, Y.Y. Zhang, A.B. Yuan, J.Q. Xu, *J. Alloys Compd*., 787 (2019) 429-439.
53. J.K. Zhao, Z.X. Wang, J.X. Wang, H.J. Guo, X.H. Li, G.C. Yan, W.H. Gui, N. Chen, *Ceram. Int.*, 44 (2018) 13341-13348.
54. P.C. Liu, L. Xiao, Y.F. Chen, H. Chen, *Ceram. Int*., 45 (2019) 18398-18405.
55. S.K. Meher, P. Justin, G.R. Rao, *Electrochim. Acta*, 55(28) (2010) 8388-8396